International Journal of Rock Mechanics & Mining Sciences 195 (2025) 106251

Contents lists available at ScienceDirect

International Journal of Rock Mechanics and Mining Sciences

journal homepage: www.elsevier.com/locate/ijrmms

Endo-exo classification of episodic rock creep in underground mines: Implications for forecasting violent rockbursts

Qinghua Lei [a,*], Daniel Francois Malan [b], Didier Sornette [c]

[a] Department of Earth Sciences, Uppsala University, Uppsala, Sweden
[b] Department of Mining Engineering, University of Pretoria, Hatfield, Pretoria, South Africa
[c] Institute of Risk Analysis, Prediction and Management, Academy for Advanced Interdisciplinary Studies, Southern University of Science and Technology, Shenzhen, China

ARTICLE INFO

Keywords:
Excavation
Rock creep
Endo-exo
Power law
Criticality
Catastrophic failure

ABSTRACT

Rock masses in deep underground environments under high in-situ stress often exhibit episodic creep behavior, driven by complex interactions between external perturbation and internal reorganization. The causes of these creep episodes and their link to potential catastrophic failure remain poorly understood. Here, we present a novel "endo-exo" framework for analyzing episodic rock creep in underground mines, capturing the interplay between exogenous triggers (e.g., blasting and excavation) and endogenous processes (e.g., damage and healing within rock masses). The underlying physical mechanism involves cascades of locally triggered rock block movements due to fracturing and sliding. We identify four fundamental types of episodic dynamics, classified by the origin of disturbance (endogenous or exogenous) and the level of criticality (subcritical or critical). All four types exhibit power law relaxations with distinct exponents: $1+\theta$ (exogenous-subcritical), $1-\theta$ (exogenous-critical), $1-2\theta$ (endogenous-critical), and 0 (endogenous-subcritical), all governed by a single parameter $0 < \theta < 1$. Our theoretical predictions are examined using the comprehensive dataset of a platinum mine in South Africa, where stopes display episodic closure behavior during successive mining operations. All creep episodes recorded can be accounted for in our classification with $\theta \approx 0.35 \pm 0.1$, providing strong validation of our theory. This θ value is interpreted in terms of a first-passage process driven by anomalous stress diffusion, represented by fractional Brownian motion or Lévy-type processes. Finally, we offer new insights into endo-exo interactions and the system's transition from episodic creep to catastrophic failure, with important implications for forecasting violent rockbursts.

1. Introduction

The ongoing green energy transition worldwide poses great new challenges for global supply chains of critical minerals that are essential for making solar panels, wind turbines and electric vehicle batteries. To achieve net-zero emissions by 2050, it is estimated that mineral inputs in 2040 must be six times greater than today's levels.[1] As shallow mineral resources become increasingly depleted, mining must inevitably extend to greater depths, which however faces substantial challenges, particularly rock mass instability under high in-situ stresses.[2–10] Extensive field observations reveal that rock masses surrounding deep mines commonly exhibit episodic creep behavior, characterized by sudden movements followed by gradual, time-dependent relaxation, typically triggered by mining or seismic activities.[11–18] In some cases, rock masses undergo episodic creep for extended periods without collapsing,[12–14,16,19] whereas in others, these episodic movements can escalate into violent rockbursts after hours to weeks of intermittent evolution.[15,20–24] The mechanisms behind these episodic creep responses and their link to potential catastrophic failure remain poorly understood, limiting our ability to forecast and mitigate violent rockburst events.

We identify three core research questions: (i) Does episodic rock creep have an exogenous or endogenous origin? (ii) What are the physical mechanisms driving these episodic movements? (iii) How do they contribute to or relate to violent rockbursts? In this context, we define exogenous (exo) triggers as external perturbations imposed on the rock mass surrounding an excavation, such as blasting operations, excavation activities, and remote seismic events, while endogenous (endo) factors refer to internal processes occurring within the rock mass

* Corresponding author.
E-mail address: qinghua.lei@geo.uu.se (Q. Lei).

https://doi.org/10.1016/j.ijrmms.2025.106251
Received 28 June 2025; Received in revised form 11 August 2025; Accepted 25 August 2025
Available online 29 August 2025

itself, such as damage accumulation, healing, internal faulting, and evolving frictional or material properties. To address these questions, we develop a novel "endo-exo" theoretical framework to quantitatively analyze the precursory and recovery patterns associated with episodic rock creep events. The rationale behind this is that complex systems like fractured rock masses composed of numerous interacting rock blocks can display distinguishable precursory and recovery characteristics in response to large fluctuations.[25] These signatures can be used to distinguish endogenous from exogenous origins of episodic dynamics—an approach that has been demonstrated for various geophysical phenomena such as earthquake sequences[26,27] and landslide movements.[28] In fact, all real-world geophysical systems are fundamentally governed by the interplay of external perturbations and internal processes, rendering the endo-exo interaction a universal phenomenon.[29] Examples include seismogenic faults,[30] volcanoes,[31] landslides,[32] glaciers,[33] and underground mines.[8] These systems are out-of-equilibrium (i.e., with macroscopic properties evolving over time) and open (i.e., interacting with their surroundings). Our foundational endo-exo theory provides a comprehensive and quantitative framework for understanding the dynamical evolution of these diverse complex geophysical systems, and offers useful diagnostic tools for distinguishing endogenous factors (i.e., internal mechanisms governing system behavior) from exogenous influences (i.e., external shocks or interventions affecting the system).

In this paper, with a specific focus on underground mines to test the endo-exo framework, we mainly study the episodic creep regime, where endogenous and exogenous origins can be distinguished, and also briefly investigate the catastrophic failure regime, which is covered more comprehensively in our previous work.[20–22,34] We provide a detailed demonstration of the endo-exo framework using the stope closure monitoring data from a tabular platinum mine in South Africa. This mine site is located at a depth of approximately 1400 m, placing it within the medium-depth mining category[35]; however, its multi-reef setting produces behavior similar to that observed under deep mining conditions. We further explore the physical mechanisms driving endo-exo interactions and the system's transition from episodic creep to catastrophic failure leading up to violent rockbursts. The insights obtained from the mine system, where underground excavations provide unique access to the source region of failure events, are not only relevant for mining safety, but are also of general and relevant interest in connection with earthquakes, landslides, volcanoes, and glaciers, where such direct access is limited or even impossible.

The remainder of the paper is organized as follows. Section 2 presents the endo-exo concept, mathematical formulations, and classification principles, as well as data acquisition and analysis methods. Section 3 reports the results, which are further discussed in Section 4. Finally, conclusions are drawn in Section 5.

2. Methodology

2.1. Problem conceptualization

Fig. 1a shows the representative configuration of a tabular excavation in underground mines,[12,15,16,36,37] where mining proceeds laterally by progressively advancing the stope faces through drilling and blasting, in a direction subparallel to the strike of the targeted ore-bearing reef.

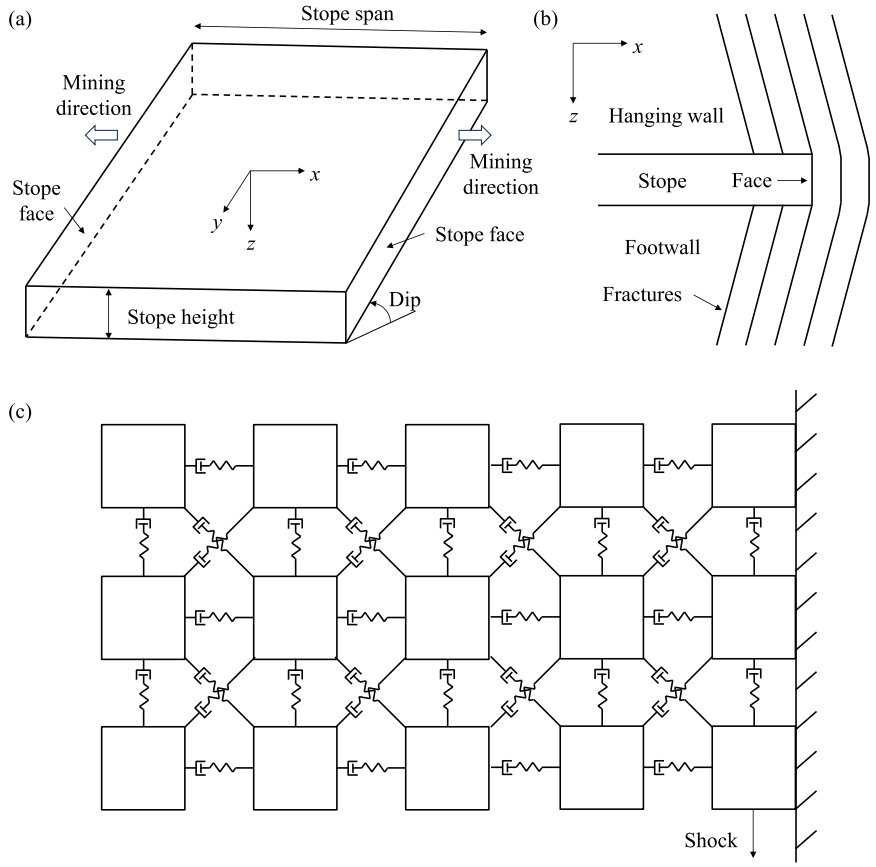

Fig. 1. (a) Schematic of a typical parallel-sided dipping tabular stope. (b) Cross-sectional view of the stope, showing subvertical fractures generated near the edges. (c) Conceptual picture of the rock mass around the stope as a complex system composed of numerous blocks interacting via cohesive or frictional contacts, with block interactions governed by a time-dependent response function (note that the diagram is for illustrative purposes only; blocks do not necessarily have equal size, the frictional interface on the right side does not have to be vertical, and the connectivity pattern between blocks may differ from that shown).

These tabular geometries are common in the gold mines of the Witwatersrand Basin (sedimentary rocks) and platinum mines of the Bushveld Complex (igneous rocks) in South Africa (see Fig. 2 for the photograph of a typical tabular platinum stope). The stope height is typically about 1–1.5 m, much smaller than the span, which may extend for several hundred meters or more. Thus, a stope excavation is often viewed as a thin slit embedded within an elastic or inelastic rock mass,[5,15,16,37] analogous to a Griffith-type crack in brittle solids.[38] High stress concentrations near the edges of an excavation in the stopes could give rise to the formation of subvertical fractures, typically extending vertically for several tens of meters and spaced at less than 1 m, which develop roughly parallel to the advancing stope faces (Fig. 1b).[5] Such a fracture zone forms within both the hanging wall above and the footwall below the stope,[5] and can extend several meters ahead of the stope face as well.[12] As the mining face advances, dislocation movements along these fracture planes may cause differential block motions in the hanging wall and footwall, which are further manifested as closure or even contact between the stope roof and floor in regions away from the face.[12,16] In this paper, the term "closure" refers to relative movement of the hanging wall and footwall. In the platinum mines, the rock mass behavior of the igneous rocks of the Bushveld Complex is dominated by multiple sets of pre-existing joints. In this case, as the mining face advances, discontinuous movements occur along the joints in the hanging wall which can lead to large panel collapses.

We conceptualize the rock mass surrounding a stope excavation as a complex system composed of numerous rock blocks interacting through cohesive and frictional contacts (Fig. 1c). This conceptual picture mirrors the classical slider block model, a simplified framework commonly used in the earthquake community to conceptualize the interplay between heterogeneity and interactions, leading to cascading events reminiscent of domino chains or avalanches.[39,40] It is also reminiscent of the classical block theory, which is well accepted in the geomechanics community for rock mass stability analysis.[41] It additionally resonates with dislocation theory modeling stope deformation as emerging from the collective interactions of dislocations within rock masses, which has been employed to study both gradual and abrupt deformations in mine stopes.[15,16] The number of blocks in the system is assumed to be large, which is justified by the small spacing between subvertical fracture planes relative to the stope span, as well as the presence of reef-parallel bedding planes in the gold mines and many intersecting joints in the platinum mines. Building upon this assumption, we establish a mean-field theoretical framework grounded in the principles of statistical physics and derive analytical solutions to approximately describe the macroscopic behavior of the complex rock block system in response to mining and related activities. Note that the specific topology of block connections does not affect the applicability of our mean-field model, as long as the number of interacting blocks is sufficiently large.

2.2. Epidemic-type triggering process

The stope closure activity arises from a combination of external forces, such as blasting and excavation, and internal effects, where each previously moved block can trigger movements of adjacent blocks through stress redistribution. This influence of a block on its nearby blocks is often not instantaneous, due to the time-dependent nature of the relevant geomechanical processes like subcritical crack growth[42] and rate- and state-dependent friction.[43] This latency can be described by a "bare" memory kernel $\phi(t-\tau)$, giving the probability that the movement of a block at time τ leads to the movement at a later time t of another block in direct interaction with the first moved block. This bare memory kernel $\phi(t-\tau)$ encapsulates the fundamental macroscopic response time governing how long it takes for a block to be triggered into motion due to its interaction with a previously activated neighbor. In other words, it describes the distribution of waiting times between cause and action for a block to move. Based on many empirical observations such as Andrade's law of material creep[44] and Omori's law of aftershock activity,[45] as well as various theoretical derivations using the constitutive laws of subcritical crack growth,[46] rate- and state-dependent friction,[47] and material rheology,[48] we assume that $\phi(t-\tau)$ takes the form of a power law that typically characterizes long-memory processes[25]:

$$\phi(t-\tau) = \frac{\theta c^{\theta}}{(t-\tau)^{1+\theta}}, \tag{1}$$

with $0 < \theta < 1$ and for $t-\tau > c$.

The exponent θ governs the decay rate of past influences, effectively setting the memory span of the interaction kernel. The constant c is a small characteristic time scale defining the onset of the power law decay and reflecting the time required for rupture[49] due to brittle creep,[50] viscous deformation,[51] pore pressure diffusion,[52] and/or frictional slip.[47] Here, the lower bound of θ ensures that $\phi(t-\tau)$ is normalisable, i.e., $\int_{\tau+c}^{+\infty} \phi(t-\tau)dt = 1$, while the upper bound is based on documented empirical data[48,53] revealing that θ rarely exceeds unity.

Let us now consider the block triggering process within the rock mass surrounding a stope excavation. Starting from an initial moved block, referred to as the "mother" block, which first moves due to either external forces (e.g., blasting) or internal fluctuations, it may trigger the movements of its first-generation neighbor "daughter" blocks, which subsequently trigger their own daughter blocks to move, continuing the cascade. We employ a mean-field approximation that represents block-to-block triggering interactions through an epidemic-type framework, modelled as a conditional self-excited point process.[54] This process has an exact mapping onto a branching process and can be mathematically described in terms of its average dynamics as[25,29]:

$$\nu(t) = V(t) + n\int_{-\infty}^{t} \phi(t-\tau)\nu(\tau)d\tau = V(t) + n\int_{-\infty}^{t} \Phi(t-\tau)V(\tau)d\tau. \tag{2}$$

Fig. 2. Photographs of a typical tabular platinum stope (left) and the hanging wall unravelling along the joints prior to a large panel collapse (right). There are many interacting blocks in the hanging wall. Note the evidence of significant closure and the broken elongates.

Here, $v(t)$ is the average closure rate (also called velocity hereafter) evolving over time t; $V(t)$ is the exogenous activation that is not triggered by any epidemic effect within the system; $\Phi(t-\tau)$ is the "dressed" or renormalized memory kernel, which encodes the effective influence of a block set exogenously in motion at time τ on subsequent triggering at time t. This kernel integrates the multi-step dynamics from the exogenous input $V(\tau)$ to the endogenous response $v(t)$, and accounts for all possible generations of triggered block motions within the resulting triggering cascade; $n \geq 0$ is the branching ratio defined as the average number of first-generation triggered daughter block motions per mother block motion. Equation (2) is the equation for the first-order moment (or average) of the velocity, whose underlying dynamics is governed by a self-excited point process.[54] The first equality in equation (2) highlights that the current velocity $v(t)$ is influenced by all prior block motions, mediated by the bare memory kernel $\phi(t-\tau)$ that governs the direct triggering within each individual mother-daughter block pair, resulting in a self-consistent integral equation. The second equality in equation (2) presents the formal solution to this integral equation since the velocity does not appear anymore in the integral term. It describes how $v(t)$ arises from all past exogenous activations $V(\tau)$ with $\tau < t$, mediated by the dressed memory kernel $\Phi(t-\tau)$, collectively incorporating all generations of block interaction cascades.

The branching ratio n depends on the network topology of the block system and the spreading behavior of disturbances within the rock mass, thereby reflecting the system's maturation. For $n < 1$, the system is in the subcritical regime,[55,56] where each block that moves induces on average fewer than one subsequent block to move in direct lineage. Consequently, the number of triggered blocks eventually decays to zero in the absence of external forcing. In this subcritical regime, the energy released by moving blocks is smaller than the energy required to trigger them. For $n > 1$, the system is in the supercritical regime,[55,56] where the number of triggered masses on average grows exponentially with time[26] or even faster.[57] In this regime, the energy released by the movement of a block typically surpasses the energy needed to initiate its movement. For $n = 1$, the system is in the critical regime, sitting at the borderline between the subcritical and supercritical regimes. In this state, the number of blocks triggered by a single block motion is distributed according to a heavy-tailed power law distribution,[58] reflecting a very large susceptibility to external shocks. In this paper, we focus on the subcritical and critical regimes with $n \leq 1$ to ensure stationarity under steady-state external forcing, whereas the supercritical regime $n > 1$ related to the occurrence of a catastrophic failure[26,28,57] will be briefly explored in Section 4.

2.3. Solutions of the mean-field equation of epidemic-type triggering process

We present the solutions of the mean-field model, equation (2), to characterize the macroscopic behavior of rock masses in response to external or internal shocks. First, let the rock mass be subjected to a strong external shock, e.g., a blasting event, where the exogenous activation $V(t)$ is represented by a Dirac function:

$$V(t) = V_c \delta(t - t_c). \tag{3}$$

Here, V_c is the amplitude of the impulse occurring at time t_c and δ is a unit impulse. Substituting equation (3) into the second integral of equation (2) yields:

$$v(t) = V_c \delta(t - t_c) + n \int_{-\infty}^{t} V_c \delta(\tau - t_c) \Phi(t - \tau) d\tau = n V_c \Phi(t - t_c), \tag{4}$$

for $t > t_c$, which indicates that the post-peak dynamics are fully governed by the dressed memory kernel $\Phi(t-\tau)$ that can be derived as the solution of the Green's function of the first equality of equation (1)[25]:

$$\Phi(t - t_c) = V_c \delta(t - t_c) + n \int_{-\infty}^{t} V_c \phi(t - \tau + t_c) \Phi(\tau - t_c) d\tau. \tag{5}$$

The solution is obtained by applying the Laplace transform to equation (5), which provides the Laplace transform of $\Phi(t-\tau)$. Taking the inverse Laplace transform then yields[26]:

$$v(t) \propto \Phi(\tau - t_c) \propto \begin{cases} 1/(t - t_c)^{1-\theta}, & \text{for } c < t - t_c < t^* \\ 1/(t - t_c)^{1+\theta}, & \text{for } t - t_c > t^* \end{cases}. \tag{6}$$

where t^* is a characteristic crossover time given by[26]:

$$t^* = c \left[\frac{n\Gamma(1-\theta)}{|1-n|} \right]^{1/\theta} \propto |1-n|^{-1/\theta}, \tag{7}$$

where $\Gamma(\cdot)$ is the gamma function. One can see that, as $n \to 1$ (in the critical regime), $t^* \to +\infty$, meaning that the early-time response ($t - t_c < t^*$) dominates; instead, if $0 < n < 1$ (in the subcritical regime), t^* has a finite value, with the system characterized by a co-existence of both early-time response ($t - t_c < t^*$, where triggering cascades thrive) and late-time response ($t - t_c > t^*$, where triggering cascades diminish).

Without a significant external event, a peak may also spontaneously arise in the velocity evolution, from the combined effect of continuous stochastic fluctuations driven by minor noisy external perturbations and an amplified sequence of epidemic cascades generated by internal interactions. The average velocity trajectory before and after the endogenous peak v_c, conditioned on the existence of this peak at time t_c, is expressed by[25]:

$$v(t|v(t_c) = v_c) \approx \frac{v_c}{\mathrm{var}(v_c)} \mathrm{cov}(v(t), v_c) = \frac{v_c}{\mathrm{var}(v_c)} \int_{-\infty}^{\min(t, t_c)} \Phi(t - \tau) \Phi(t_c - \tau) d\tau, \tag{8}$$

for both $t < t_c$ and $t > t_c$. Considering equation (6), we can finally obtain:

$$v(t) \propto 1 \Big/ (t - t_c)^{1-2\theta}, \tag{9}$$

for $c < |t - t_c| < t^*$ or equivalently for $n \to 1$.

For $n < 1$ (subcritical regime), the system's response is primarily driven by random fluctuations, behaving essentially as a noise process, and can be described by:

$$v(t) \propto 1 \Big/ |t - t_c|^0, \text{ for } |t - t_c| > t^*. \tag{10}$$

2.4. Endo-exo classification

Based on the solutions derived above, the stope closure velocities near a peak at time t_c can be represented by a generalized power law finite-time singularity function:

$$v(t) \propto 1 / |t - t_c|^p, \tag{11}$$

where the exponent p depends on the parameter θ and the regime delineated by the characteristic crossover time t^*. This framework enables classification of velocity peaks into four distinct types (Fig. 3), distinguished by the origin of disturbance (endogenous versus exogenous) and the level of criticality (subcritical versus critical):

- Exogenous-subcritical peak ($n < 1$ and $t - t_c > t^*$), characterized by $p = 1 + \theta$. In this case, the cascading propensity is limited ($n < 1$), and the exogenously induced velocity jump at time t_c does not cascade beyond the first few generations of triggered blocks (Fig. 3a). The snapshots in Fig. 3a show blocks (blue) whose activity rapidly diminishes after t_c, with the activity of some triggered blocks (yellow) appearing briefly before disappearing, indicative of short-lived cascades.

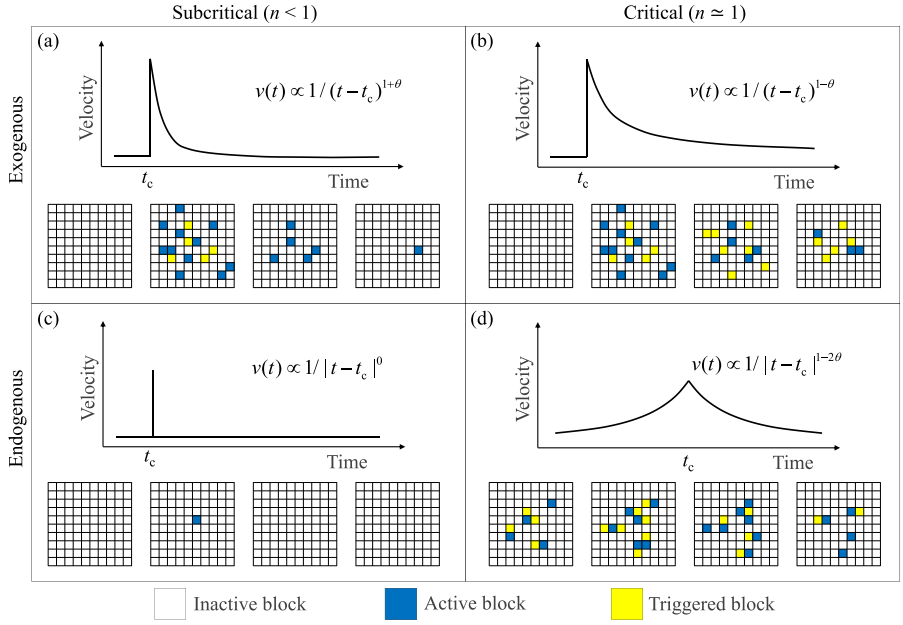

Fig. 3. Classification of episodic creep dynamics based on the origin of disturbance (endogenous versus exogenous) and the level of criticality (subcritical versus critical). There are four distinct types of power law velocity dynamics $v(t)$ around a peak at time t_c and they are all related to a single parameter θ. The series of snapshots below each velocity trajectory illustrates the evolution of triggering processes within a rock block system (with inactive blocks, active blocks, and triggered blocks color-coded) underpinning the velocity time history. (For interpretation of the references to color in this figure legend, the reader is referred to the Web version of this article.)

- Exogenous-critical peak ($n \approx 1$ and $c < t-t_c < t^*$), characterized by $p = 1-\theta$. In this case, the system is in a critical state ($n \approx 1$), such that the exogenously induced velocity jump at time t_c cascades throughout the block system, where activated blocks trigger further movements of their neighbors, and so forth (Fig. 3b). The snapshots in Fig. 3b show newly triggered blocks (yellow) propagating outward over time, resulting in sustained, far-reaching cascades that extend beyond the initially active zones (blue).
- Endogenous-subcritical peak ($n < 1$ and $|t-t_c| > t^*$), characterized by $p = 0$. The closure activity arises not from an external shock but from endogenous interactions. Limited cascading occurs ($n < 1$), resulting in a velocity peak that lacks apparent precursory or recovery signatures (Fig. 3c). The snapshots in Fig. 3c show an anomalously active block (blue) with no triggered blocks (yellow), illustrating the isolated nature of the endogenous-subcritical peak.
- Endogenous-critical peak ($n \approx 1$ and $c < |t-t_c| < t^*$), characterized by $p = 1-2\theta$. Here, the closure activity arises from endogenous growth and interaction within a critical system ($n \approx 1$), leading to movement cascades that exhibit an approximately symmetrical power law acceleration and deceleration patterns around the peak (Fig. 3d). The snapshots in Fig. 3d reveal a wave of active blocks (blue), continuously replenished by triggered blocks (yellow), progressively building up before t_c and gradually decaying afterward.

This classification of system responses into four qualitatively distinct regimes emerges from the interplay of the long-memory process as described by equation (1) and the mean-field epidemic cascade throughout the system as captured by equation (2). The four peak types, characterized by distinct power law exponents $1+\theta$, $1-\theta$, 0, and $1-2\theta$, are all governed by a single parameter θ, highlighting the unifying nature of our classification. It can be seen that the recovery following an endogenous-critical peak (with a smaller exponent $p = 1-2\theta$) is slower than that following an exogenous-critical peak (with a larger exponent $p = 1-\theta$). This more persistent influence of an endogenous-critical peak results from its longer precursory preparation, which permeates the system more deeply than an exogenous-critical peak. Note that exogenous peaks do not exhibit apparent precursors (see Fig. 3a and b), as they are triggered by external events that impose sudden shocks to the system. Based on this taxonomy, velocity peaks can be readily classified based on their distinct precursory and recovery patterns. Specifically, exogenous peaks exhibit power law relaxation without apparent precursory acceleration, with exogenous-critical peaks having $p < 1$ and exogenous-subcritical ones having $p > 1$; on the other hand, endogenous critical peaks are characterized by symmetrical power law acceleration and deceleration with $p < 1$, while endogenous subcritical peaks exhibit no apparent precursory and recovery dynamics with p being around 0. Thus, the distinct characteristics of each peak type enable differentiation between endogenous versus exogenous origins of episodic rock creep, based on the system's dynamical response around peaks rather than potentially ambiguous correlations with external events. It is important to clarify that the differentiation here pertains to the initial triggering source (whether internal or external), rather than the internal mechanisms of the system's response, which are always governed by endogenous self-excited triggering processes within the rock mass. It is also worth emphasizing that the endo-exo framework applies to the subcritical and critical regimes (e.g., episodic creep), where endogenous and exogenous origins of velocity peaks can be distinguished. The assumption of linearity and additivity underlying the current mean-field formulation would break down for the supercritical regime (e.g., catastrophic failure), where the system response is characterized by an entangled endo-exo origin.

Using the epidemic response function model as a unified classification framework provides a simple yet powerful lens for understanding the apparently diverse large-scale responses of the system, with the single exponent θ governing all regimes. However, this does not imply that local variations are unimportant. When the goal is to characterize local complexity and heterogeneity in detail, additional parameters or spatially resolved models are necessary to capture those effects. While our statistical physics-based model is primarily a phenomenological approach, it complements traditional fracture mechanics and elastic-plastic mechanics by providing a macroscopic description of event cascades emerging from complex block interactions. The micromechanical

mechanisms underlying these triggering and cascading phenomena relate to processes such as stress redistributions and progressive damage accumulation in rock masses. Integrating these perspectives constitutes a valuable direction for future work.

2.5. Data acquisition and analysis approach

We conduct a comprehensive case study to test the endo-exo theory using stope closure measurements from a platinum mine in South Africa, where multiple panels mined within the Upper Group 2 (UG2) reef at a depth of approximately 1400 m below the ground surface.[13] The UG2 reef is a chromitite layer within the Bushveld Complex, one of the world's largest layered mafic intrusions, renowned for its high concentrations of platinum group metals including platinum, palladium, and rhodium. The UG2 panels were mined beneath the Merensky Reef (see Fig. S1 in the Supplementary Material for the layout of UG2 panels), another platinum-rich layer within the Bushveld Complex that had been previously exploited in this region. As UG2 mining approached and extended beneath the Merensky remnant, significant closure occurred within the extending stope, which was closely monitored at multiple panels using clockwork closure meters instrumented between the hanging wall and footwall.[13] Such closure meters can continuously record stope closure, providing measurements as a function of time at a sampling frequency significantly greater than that of mining face advance cycles[13,14,59] (see Fig. S2 in the Supplementary Material for the field setup and operational mechanisms of the closure meters instrumented). These stope closure measurements collected at the site scale constitute valuable real-world field data that will be used to rigorously examine and validate (or falsify) our endo-exo theoretical framework.

We derive velocity time series $v(t)$ by differentiating the closure time series with respect to time. Subsequently, we fit the velocity data around a peak to the following equation:

$$v(t) = \frac{C}{(t - t_c)^p} + v_r, \tag{12}$$

where C is a constant and v_r is the residual velocity when the system has fully recovered from external perturbations. The determination of this residual velocity for a stope during mining is subject to uncertainties, because the rock mass has very rare opportunities to completely recover from an external perturbation (e.g., blasting operations, excavation activities, and seismic events) before the next event occurs. Here, we estimate the residual velocity by first detecting troughs in the velocity time series and then define the residual velocity associated with a given peak as the minimum of the two nearest troughs (with one before the peak and one after the peak). This residual velocity is found typically around 3×10^{-5} mm/min in our analysis, which is compatible with past field observations of near-zero closure rate during the December holidays when blasting and excavation cease in the mine. Although this method is simple, sensitivity tests varying the residual velocity within relevant ranges demonstrate a negligible impact on the results of our model calibration, thereby supporting the robustness of our analysis. To estimate C and p, we use the least square method to minimize the sum of squared errors:

$$s = \sum_{t_i} \varepsilon(t_i)^2 = \sum_{t_i} \{\ln[v(t_i) - v_r] - \ln C + p \ln|t_i - t_c|\}^2, \tag{13}$$

where $v(t_i)$ is the empirically measured velocity at time t_i. We then set the partial derivatives $\partial s/\partial(\ln C)$ and $\partial s/\partial p$ to be both equal to zero, leading to solve a linear system of two equations with the two unknowns C and p. Thus, through the least squares method, we can fit equation (12) to the time series of net velocity $v(t) - v_r$ around each peak to estimate the associated power law exponent p, with its standard deviation derived from the confidence interval of the fit. Unless stated otherwise, velocity in the following sections refers to the net velocity.

3. Results

Fig. 4a and 5a present the closure measurements for UG2 Panel 1N (where "1" denotes the panel number and "N" indicates the northern sector of mining), mined toward the Merensky remnant (see Fig. S3 in the Supplementary Material for the location of Panel 1N with respect to this remnant), from June to August 2005. During this period, the face advanced 23.1 m in total, such that part of the UG2 face reached beneath the boundary of the Merensky remnant. The data shown in Fig. 4a and 5a were recorded at two different locations, as the closure meter was relocated closer to the advancing face on August 3, 2005. The stope displayed a step-like deformation pattern over time, marked by multiple episodes of temporary acceleration and deceleration (Fig. 4a and 5a). Notably, significant jumps in closure occurred immediately after each blasting event, followed by a gradual deceleration sustained over time. Post-peak velocity relaxation following these blast-induced exogenous-critical peaks obeys a power law, with an exponent of $p = 0.54 \pm 0.03$ at the first measurement position (Fig. 4b) and $p = 0.57 \pm 0.20$ at the second position (Fig. 5b). These p values generally show a good agreement, but a more pronounced dispersion is observed in the data collected at the second position, likely due to its closer proximity to the Merensky remnant and the resulting stronger stress redistribution and/or more heterogeneous ground response. This may also account for the significantly higher closure rate at the second measurement position, where almost 120 mm of closure was reached over 17 days (Fig. 5a), compared to around 140 mm over 40 days at the first position (Fig. 4a). The panel remained stable despite such high rates of closure (see Fig. S4 in the Supplementary Material for a field photo of this panel).

We further analyze the closure data collected for UG2 Panel 4S (where "4" denotes the panel number and "S" indicates the southern sector of mining) over a 35-day period from September 21 to October 26, 2005 (Fig. 6). The panel was already situated below the Merensky remnant when the monitoring began (see Fig. S5 in the Supplementary Material for the panel location). During the monitoring period, the face advanced 14.1 m in total. The stope also exhibited a step-like deformation pattern over time, characterized by a series of acceleration-deceleration episodes associated with successive blasting operations (Fig. 6a). Post-peak velocity relaxation following these blast-induced exogenous-critical peaks obeys a power law, with an exponent of $p = 0.69 \pm 0.07$ (Fig. 6b). In addition to those blast-induced acceleration-deceleration sequences, an acceleration crisis spontaneously emerged on October 17, 2005, in the absence of any blasting event (Fig. 6c). This coincided with a catastrophic failure event in the adjacent Panel S5 (see Fig. S6 in the Supplementary Material for a photo of this collapse) and was followed by a gradual deceleration over the next few days (Fig. 6c). This endogenous-critical peak appears to be preceded by a progressively accelerating power law growth of velocity and succeeded by an approximately symmetrical power law decline of velocity, which are characterized in general by a common exponent of $p = 0.36 \pm 0.06$ (Fig. 6d). Note that only two data points are available for the pre-peak stage, while earlier velocities show no correlation with the peak, possibly because this endogenous-critical event originated in the adjacent Panel S5 and had not yet influenced Panel 4S at that time.

Fig. 7a shows the closure behavior recorded at the first measurement position in UG2 Panel 6N for the period from January 24 to February 5, 2007, during which the face advanced 7.8 m. The post-peak velocity relaxation following blast-induced exogenous peaks also conforms to a power law, with an exponent of $p = 0.56 \pm 0.07$ (Fig. 7b). An acceleration crisis developed on February 01, 2007, during which an abrupt jump in closure was observed (Fig. 7c). The corresponding velocity peak is surrounded by an essentially noisy stationary velocity trajectory with no apparent precursory and recovery trends, with the power law exponent p close to 0 (Fig. 7d), thus manifesting as an endogenous-subcritical peak.

Fig. 8a further presents the closure data collected at the second measurement position in UG2 Panel 6N from February 9 to February 11,

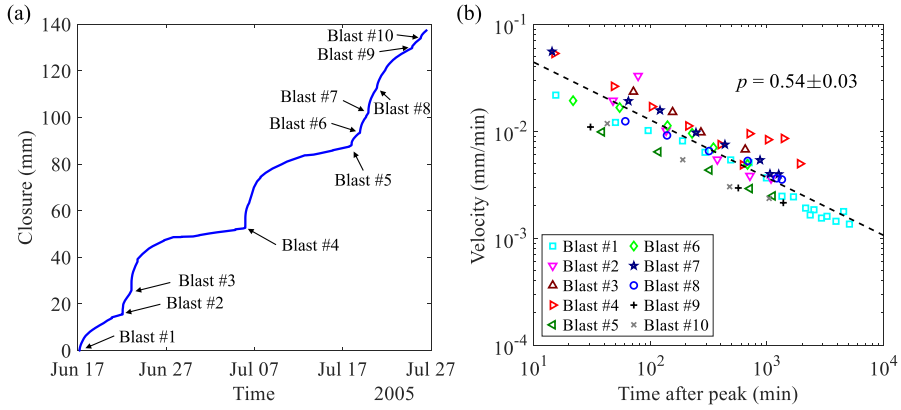

Fig. 4. (a) Closure measurements at the first instrumentation position for UG2 Panel 1N during the period from June 17 to July 27, 2005. The start and end of the time series respectively correspond to distances of 9.4 m and 20.0 m from the advancing stope face. (b) Post-peak velocity relaxation following blast-induced exogeneous-critical peaks, with the dashed line indicating the power law fit.

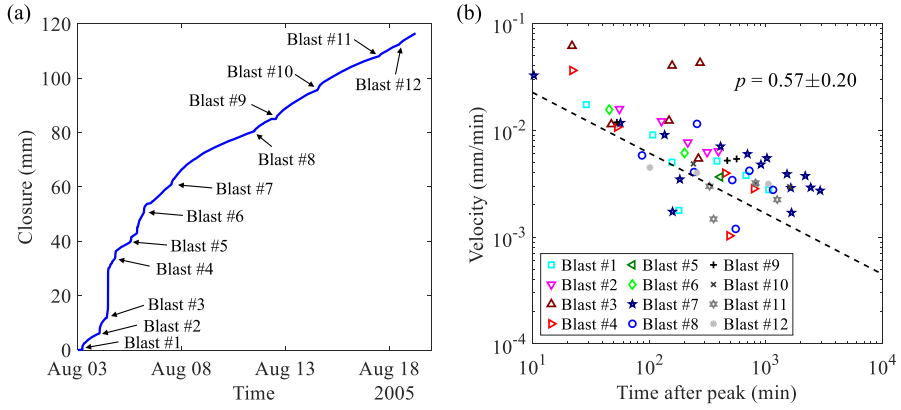

Fig. 5. (a) Closure measurements at the second instrumentation position for UG2 Panel 1N during the period from August 03 to August 19, 2005. The start and end of the time series respectively correspond to distances of 11.8 m and 24.3 m from the advancing stope face. (b) Post-peak velocity relaxation following blast-induced exogeneous-critical peaks, with the dashed line indicating the power law fit.

2007. During this short period, the face advanced 2 m before the panel was abandoned due to the high closure rate encountered as it reached beneath the Merensky remnant. Interestingly, the velocity relaxation following blast #1 exhibits a two-branch power law scaling behavior: the early-time response within approximately 100 min is characterized by an exponent $p = 0.76 \pm 0.36$, while the late-time response is associated with $p = 1.35 \pm 0.11$ (Fig. 8b). These characteristics indicate that it is an exogenous-subcritical peak. On the other hand, the velocity recovery following blast #2 exhibits a single power law trend with an exponent $p = 0.66 \pm 0.05$ (Fig. 8b), indicating that it is an exogenous-critical peak.

Thus, all the four types of episodic rock creep, namely endogenous/exogenous-subcritical/critical, have been found in the closure measurement data. Interpreting these results in light of equations (6), (9) and (10), the various exponents p in expression (12) can be mapped onto $1+\theta$, $1-\theta$, 0, or $1-2\theta$ and can thus be associated with the four distinct types of velocity peaks. Remarkably, all these exponents emerge naturally from the endo-exo framework and depend solely on a single parameter $\theta \approx 0.35 \pm 0.1$. These results provide a strong validation of our endo-exo theoretical framework. We acknowledge that some velocity peaks, particularly the endogenous ones, are derived from limited data, and individual fits may sometimes have limited reliability due to data sparsity or measurement noise. However, it is important to emphasize that our framework is a mean-field model designed to capture the average macroscopic behavior of the system rather than local variations. Consequently, classification and parameter estimation should primarily focus on the mean trends observed across different datasets. The scatter observed among individual fits reflects the inherent heterogeneity of the real system and does not undermine the validity of our model, since the mean trends remain well captured. While individual fits may vary in precision due to data limitations and noise, the overall consistency across multiple closure datasets supports the reliability of the θ estimate and the robustness of the classification framework.

4. Discussion

4.1. Mechanisms behind the observed parameter θ

We have developed an endo-exo framework for the analysis of episodic rock creep in underground mines. It offers a quantitative classification of episodic rock creep into four fundamental types, each with distinct precursory and recovery signatures, yet all coherently explained by a single epidemic response function model whose remarkable explanatory power lies in capturing every regime through different power law response functions governed by the same single parameter θ. All four power law regimes of episodic dynamics were found in the data from a platinum mine in South Africa, yielding $\theta \approx 0.35$, which is notably smaller than the value of 0.5 predicted by a random stress model assuming normal diffusion of stress fluctuations.[28,60] To reconcile this difference, we extend the random stress model to account for anomalous stress diffusion with persistent or bursty stress fluctuations, producing a

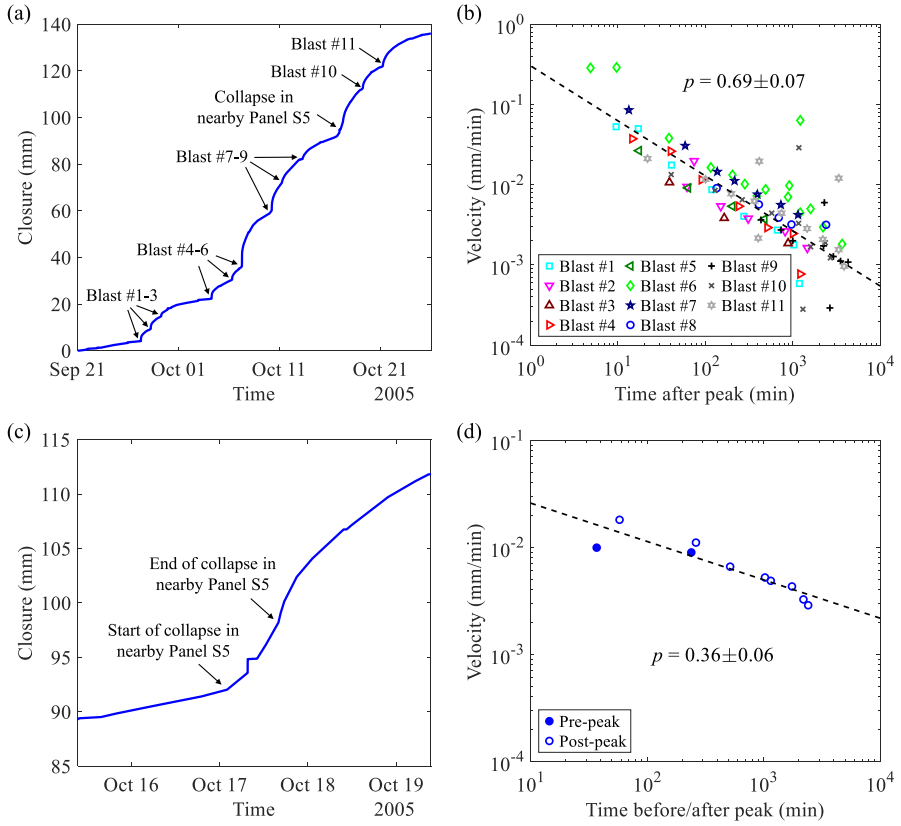

Fig. 6. (a) Closure measurements for UG2 Panel 4S during the period from September 21 to October 26, 2005. The start and end of the time series respectively correspond to distances of 7.4 m and 21.5 m from the advancing stope face. (b) Velocity relaxation following blast-induced exogeneous-critical peaks, with the dashed line indicating the power law fit. (c) Local view of the closure curve around an endogenous acceleration crisis during which the adjacent Panel S5 experienced a collapse. (d) Pre-peak acceleration and post-peak relaxation of velocity around an endogenous-critical peak, with the dashed line indicating the power law fit.

power law form of the bare memory kernel $\phi(t)$ with θ matching the observed value. Specifically, we consider two plausible mechanisms: (i) fractional Brownian motion—a non-Markovian process with correlated stress fluctuations, and (ii) quasi-Lévy flight—a Markovian process characterized by a heavy-tailed distribution of stress jumps in the finite-variance regime.

Without loss of generality, let us adopt a dimensionless form and consider that, at time $t = 0$, a mother block moves and perturbs its neighboring first-generation daughter blocks, which are initially subject to a stress level S_0 marginally below the critical threshold S_c required to trigger movement. Suppose that the subsequent stress at each first-generation daughter block fluctuates due to random increments s originating from various possible sources (e.g., microcracking, stress redistribution, microseismic tremors), which may be described by a fractional Brownian random walk[61] associated with a Hurst exponent $0 < H < 1$ and a characteristic increment amplitude s^*. For $H = 0.5$, stress fluctuations follow normal diffusion, whereas $H \neq 0.5$ leads to anomalous diffusion with positively correlated increments for $H > 0.5$ (persistent behavior) and negatively correlated increments for $H < 0.5$ (anti-persistent behavior). Then, the waiting time for a daughter block to start moving is determined by the first-passage time of its stress $S(t)$ exceeding S_c, with the probability density function asymptotically following a power law[62,63] $\phi(t) \propto 1/t^{(2-H)}$. Comparing with equation (1) gives $\theta = 1-H$, which is confirmed by random walk simulations with parameters $S_0 = 0.9$, $S_c = 1$, $s^* = 0.01$, and $H = 0.65$, yielding $\theta = 0.35 \pm 0.02$ (Fig. 9a). Here, $S_0 = 0.9$ is chosen to reflect the near-critical stress condition expected for the rock mass surrounding the mine[5,64–66]; consistent results are also obtained for $S_0 = 0.8$, 0.85, and 0.95 (see Fig. S8–S10 in the Supplementary Material). Physically, $\theta = 0.35$ reflects persistent (positively correlated) stress fluctuations, where stress increments follow a non-Markovian process and are more likely to continue in the same direction, either towards the critical threshold or away from it. This behavior captures a memory effect in stress evolution, driven by processes such as microcrack coalescence, localized stress redistributions, and coherent microseismic perturbations. Consequently, the waiting times for daughter blocks to move are broadly distributed, with intermittent bursts of correlated stress accumulation driving block movements.

We test another random walk model whose increments s now follow a Markovian process but are drawn from a Pareto distribution $\mathbb{P}(s) = \mu s_{\min}^{\mu}/s^{\mu+1}$, where μ is the shape parameter (power law exponent) and $s_{\min}$ is the minimum increment size. For $0 < \mu < 2$, the increments of the random walk have an infinite variance and the first passage is dominated by rare large jumps that grow larger and larger over time, scaling as $s_{\max} \sim s_{\min}\, t^{1/\mu}$. As a result, the first-passage time follows the Lévy regime scaling[67] $\phi(t) \propto 1/t^{1+1/\mu}$. A comparison with equation (1) gives $\theta = 1/\mu$. For $\mu > 2$, the increments of the random walk have finite mean and variance, so the leading scaling properties of the random walk converge to those of standard Brownian motion, in accordance with the central limit theorem.[56] Consequently, the first-passage time distribution scales asymptotically as $\phi(t) \propto 1/t^{3/2}$ with $\theta = 0.5$ to leading order.[68] Nevertheless, due to the fat-tailed nature of the Pareto distribution governing stress increments, convergence to the scaling laws of the standard Brownian motion is markedly slow. This is because rare large jumps continue to significantly influence stress evolution at intermediate times, before the central limit theorem fully takes effect.[56] This gives rise to a quasi-Lévy regime in the first-passage time distribution at intermediate times. We anticipate the crossover time from this intermediate-time quasi-Lévy regime to the long-time Brownian regime to be approximately $t_{\text{cross}} \approx [(S_c - S_0)/s_{\min}]^{\mu}$, based on the criterion that

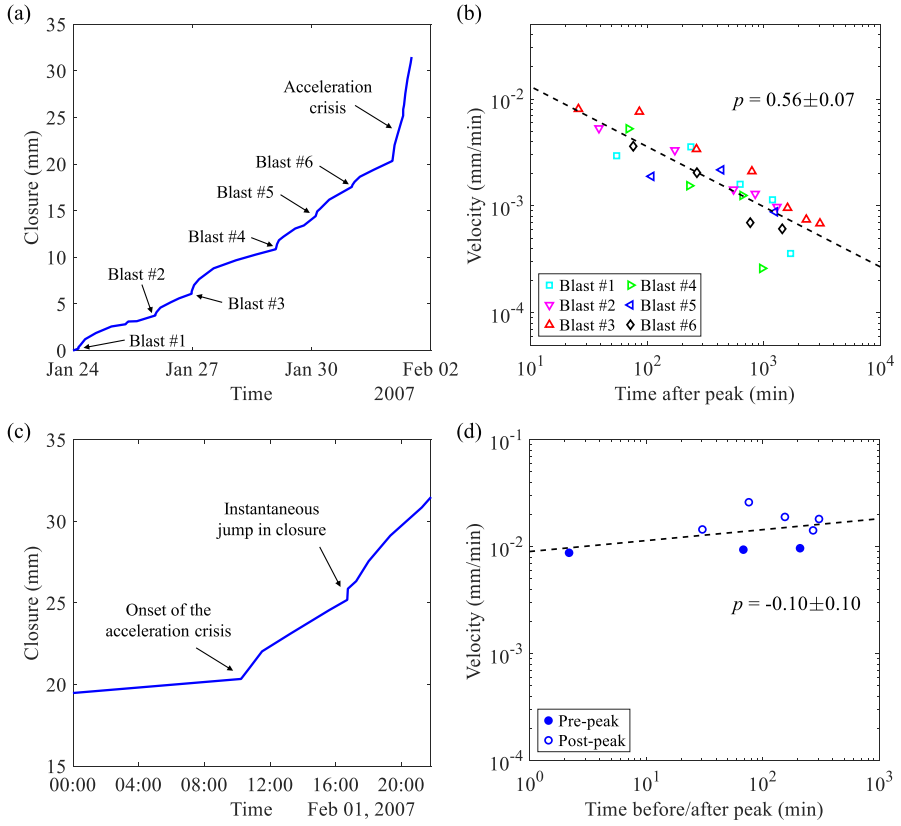

Fig. 7. (a) Closure measurements at the first instrumentation position for UG2 Panel 6N during the period from January 24 to February 05, 2007. The start and end of the time series respectively correspond to distances of 17.8 m and 25.6 m from the advancing stope face. (b) Velocity relaxation following blast-induced exogeneous-critical peaks, with the dashed line indicating the power law fit. (c) Local view of the closure curve during an acceleration crisis. (d) Pre-peak and post-peak velocity dynamics around an endogenous-subcritical peak, with the dashed line indicating the power law fit.

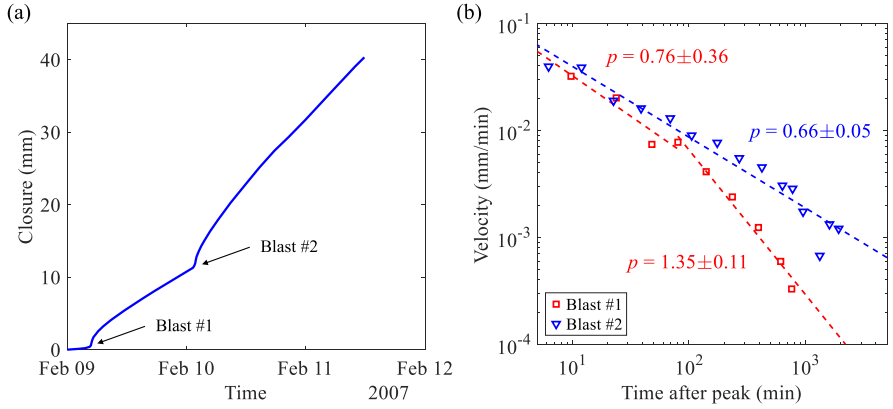

Fig. 8. (a) Closure measurements at the second instrumentation position for UG2 Panel 6N during the period from January 09 to February 11, 2007. The start and end of the time series respectively correspond to distances of 19.6 m and 21.6 m from the advancing stope face. (b) Velocity relaxation following blast-induced exogeneous-critical/subcritical peaks, with the dashed line indicating the power law fit.

the typical maximum jump s_{max} must be sufficiently large to span the threshold distance $S_c - S_0$. Random walk simulations using $S_0 = 0.9$, $S_c = 1$, $\mu = 2.86$, and $s_{min} = 0.01$ (yielding an estimated $t_{cross} \approx 724$) confirm the existence of this intermediate quasi-Lévy regime. A power law fit to the waiting time distribution up to $t = 1000$ yields $\theta = 1/\mu = 0.35 \pm 0.02$ (Fig. 9b; consistent results are also obtained for $S_0 = 0.8$, 0.85, and 0.95 as shown in Fig. S8–S10 in the Supplementary Material). This result suggests that the observed $\theta = 0.35$ in the studied platinum mine may alternatively arise from the intermittent and bursty nature of stress evolution within rock masses, driven by Lévy-type sudden and significant stress redistributions associated with microcracking or microslip events.

It is worth noting that the above random walk models also provide a natural interpretation for the parameter c in the bare memory kernel as defined by equation (1). Specifically, parameter c represents the characteristic time scale over which random walkers bridge the gap between the initial stress level and the critical threshold. Accordingly, a smaller gap corresponds to a lower c value.

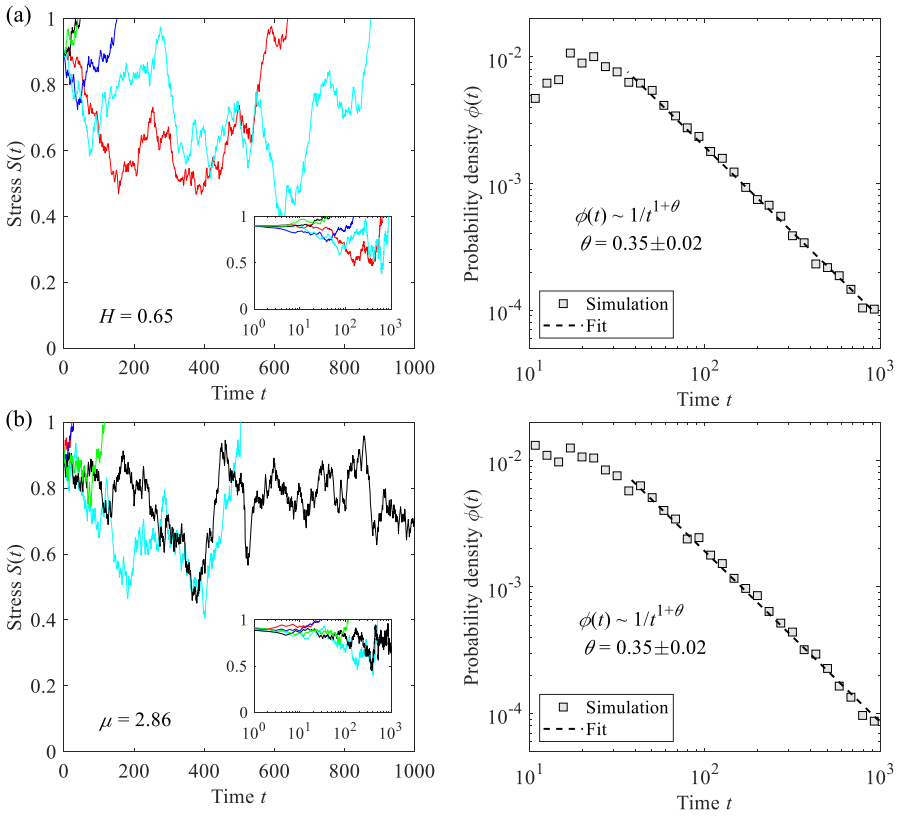

Fig. 9. Random walk simulations of stress fluctuations with increments s (a) obeying a fractional Brownian motion with a Hurst exponent of $H = 0.65$ and a characteristic increment amplitude of $s^* = 0.01$, or (b) drawn from a Pareto distribution with a shape parameter of $\mu = 2.86$ and a minimum increment size of $s_{\min} = 0.01$. In the simulation, stress $S(t)$ evolves as a random walk starting from an initial value $S_0 = 0.9$ with each step taking a unit time, and the process stops until $S(t)$ for the first time exceeds the critical threshold $S_c = 1.0$. Left panels give the stress trajectories of 5 realizations which are arbitrarily selected from 10000 simulated realizations; the inset displays the same data with a logarithmic time scale. Right panels show the probability density function of waiting times $\phi(t) \propto 1/t^{1+\theta}$, derived from the random walk simulations, with $\theta = 0.35$ obtained for both models.

4.2. *Further insights into endo-exo interactions*

Our results indicate that most large velocity peaks in this platinum mine dataset are exogenous-critical, suggesting that the rock mass around the mining stope is often in a critical state. This is consistent with previous conjectures and observations that rock masses in tabular mines are subject to high stress concentrations, particularly in the vicinity of the stope face, and are often critically (or near-critically) stressed.[5,64–66] Under such critical conditions, the rock mass response to strong external blasting events is primarily driven by cascades of triggered block movements where each triggered block motion in turn initiates the movement of subsequent blocks across multiple generations of triggering.

We have also identified an exogenous-subcritical creep event (Fig. 8b) that initially undergoes approximately 100 min of slower exogenous-critical relaxation before transitioning into a faster exogenous-subcritical phase. Substituting this characteristic time $t^* \approx 100$ min together with $\theta \approx 0.35$ and an estimate of $c \approx 1$–10 min into equation (7), we obtain $n \approx 0.62$–0.78. Here, our estimate of c is based on an inspection of the power law decay trends around peaks in the data, and it falls within the typical range of minutes to days reported in the literature.[26,45] This comparatively low branching ratio n indicates that, although the rock mass around a mining stope is often critically stressed, it may not always remain at criticality. Similar observations have been reported recently for other systems, such as earthquake faults[69] and landslides.[28] This is in contradiction with the conventional concept of self-organized criticality,[70] which postulates that the crustal rock is permanently evolving at a critical state and all the events are generated by the same underlying process, making the prediction of large events impossible. More sophisticated models of self-organized criticality have overturned this view, revealing that the stress field typically remains far from its rupture threshold.[71,72] Our results confirm the existence of different regimes, with characteristic signatures emerging during transitions that may signal the approach of catastrophic events, an insight with significant potential for improving predictive capabilities. Notably, the exogenous-subcritical peak at Panel 6N was preceded by multiple exogenous-critical peaks (Fig. 7) and then followed by an exogenous-critical peak (Fig. 8), after which the stope was abandoned due to hazardous conditions associated with high closure rates.[13] This reflects the inherently intermittent and fluctuating nature of the deep mine system, where transitions between critical and subcritical states likely arise from local heterogeneities, stress redistributions, and transient external perturbations that temporarily reduce the system's susceptibility, driving it into a brief subcritical phase. Subsequently, stress re-accumulation and cascading block movements restore critical conditions. This resonates with previous field observations reporting a slight arrest in the rate of closure or tilt before major events.[5,18] Such a dynamical, non-stationary behavior reveals the system's intrinsic complexity and highlights the necessity of continuous monitoring to provide valuable early-warning signals for hazard mitigation, as also emphasized in other studies.[13,14]

In addition, the dataset reveals the presence of endogenous-critical and endogenous-subcritical peaks (Fig. 6b and 7d), although they are much less prominent than the exogenous peaks, suggesting that these endogenous events are either rare or overshadowed by the more dramatic exogenous events. Notably, the endogenous-critical peak at UG2

Panel 4S coincided with the collapse in the adjacent Panel 5S, implying a strong endogenous coupling of the rock masses across the panels. Interestingly, similar creep episodes, lacking any apparent exogenous triggers yet exhibiting clear acceleration-deceleration trends, were previously also observed in the tiltmeter measurements at a deep gold mine in South Africa.[18] These episodes, typically lasting several days, were previously termed "anomalous" tilt in the literature[18] due to the limited understanding of their underlying mechanisms. Within our endo-exo framework, they can be rationalized as manifestations of endogenous-critical creep dynamics.

4.3. Implications for forecasting violent rockbursts

Hitherto, our focus has been primarily on the "endo-exo" regime, where rock masses exhibit repeated episodes of acceleration and deceleration, driven by the interplay of exogenous perturbation and endogenous maturation. We now explore the last research question raised in Section 1: How does episodic rock creep relate to violent rockbursts? Previous studies have proposed various theoretical models to describe episodic rock creep[12,16,37,73] and rockbursts[15,24] largely as separate phenomena, with limited attempts to connect them. Although stope closure has long been recognized and monitored as a potential precursor to rockbursts,[13,14] the underlying mechanisms linking episodic creep to catastrophic failure remain poorly understood.

As the stope excavation progresses, the surrounding rock masses may undergo a transition into the supercritical regime. This transition often arises due to endogenous maturation of the system,[29] explaining why sometimes stope collapses occur in the absence of significant blasting or seismic activities.[13] In this supercritical regime, the system dynamics typically follows the so-called Voight's equation[74,75]:

$$\dot{v}(t) \propto v(t)^{\alpha}, \text{with } \alpha > 1, \tag{14}$$

where the exponent α characterizes the degree of nonlinearity, and the condition $\alpha > 1$ ensures the presence of positive feedbacks, resulting in a finite-time singularity. This singular behavior can be seen by integrating equation (14), leading to Ref. 21:

$$v(t) \propto 1 / (t_c - t)^{p}, \text{with } p > 0, \tag{15}$$

which is in the same form as equation (11) (but only valid for $t < t_c$) with exponent $p = 1/(\alpha - 1)$ and t_c being the critical time of failure. A further integration of equation (15) gives the solution[21] of the time-dependent stope closure $\Omega(t)$:

$$\Omega(t) = A + B(t_c - t)^{m}, \text{with } m < 1, \tag{16}$$

where A and B are constants, and $m = 1 - p$ is the singularity exponent.

Such finite-time singular behavior arises in the mean-field epidemic-type formulation (2) when variations in the fertility of triggering blocks are taken into account by extending the current endo-exo framework. Mathematically, this corresponds to augmenting the bare memory kernel $\phi(t-\tau)$ defined in equation (1), with a fertility factor that quantifies the number of block motions triggered by a given initiating event. When fertilities follow a power law distribution with an exponent less than 1, the average branching ratio diverges. As shown in the previous study,[57] this leads to the finite-time singular behavior described by expression (15).

We analyze the closure measurements from UG2 Panel 7N, where a catastrophic failure event occurred on April 04, 2007 (see Fig. S7 in the Supplementary Material for a field photo of this collapse) and the system's acceleration toward the final failure was well captured by the monitoring system (Fig. 10a). We fit the pre-failure velocity time series to equation (15), obtaining $p = 0.91 \pm 0.22$ (Fig. 10b), which is generally compatible with the theoretical prediction[57] of $p = 1$ for $\theta > 0$. Independently, we fit the pre-failure closure time series to equation (16), yielding $m = 0.12$ (Fig. 10a, inset). Notably, these values approximately satisfy the expected relationship of $m = 1 - p$. From them, we can further estimate $\alpha \approx 2.1$ (equation (14)), which aligns well with the typical α values of around 2 reported in the literature.[74–76] This suggests that positive feedbacks indeed dominate the rock mass behavior as it approaches the final failure. Such positive feedbacks may arise from crack growth in intact rocks[77–80] and frictional instability along fault planes,[81,82] both of which have been documented in field observations at deep mines,[5,8,15,83–85] with the former mechanism generating smaller events and the latter one producing relatively larger events.[86]

Different from the subcritical and critical regimes for which the endo-exo classification applies, when the system enters the supercritical regime ($n > 1$), an initial exogenous shock will cascade into a dominant endogenous dynamics, carrying a finite probability of triggering cascades of events whose number grows exponentially with time[26] or even faster.[57] It is crucial to note that the underlying driving mechanisms remain the same as that in the subcritical and critical regimes: self-excitation and triggering processes. In this supercritical regime, different parts of the system are strongly coupled and interdependent,[87,88] leading to the dominance of endogenous processes. In this regime, the system is characterized by high endogeneity, making it inherently fragile and sensitive to external perturbations. Even a minor external perturbation can trigger substantial amplification through endogenous positive feedback mechanisms, leading to catastrophic failure. It is worth noting that the dramatic response of the system to a shock does not mean that the exogenous factor itself becomes more significant; rather, it is the endogenous processes that grow increasingly important, amplifying the impact of an external event on the system and

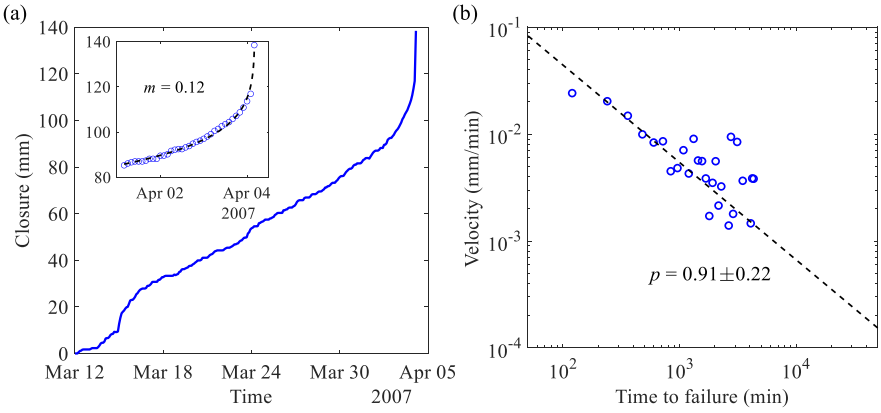

Fig. 10. (a) Closure measurements for UG2 Panel 7N during the period from March 12 to April 04, 2007. The end of the time series corresponds the occurrence of a catastrophic collapse. Inset: a zoomed-in view of closure evolution during the terminal phase prior to the final failure with the dashed line indicating the fit to the power law singularity model. (b) Pre-failure velocity as a function of time to failure (time flows from right to left), with the dashed line indicating the power law fit.

giving the illusory impression of a stronger exogenous influence.

The physical processes underlying the transition from the subcritical/critical regimes to the supercritical regime, which ultimately leads to catastrophic failures, may be related to damage accumulation under fatigue loading from repeated blasting operations and continued stope excavations. This endogenously driven failure can emit precursory signals, such as accelerated creep and log-periodic oscillations,[20–22] which are highly informative for prediction, rendering violent rockbursts potentially predictable "dragon-kings" (a double metaphor for an event of a predominant impact like a "king" and born from a unique origin like a "dragon").[88,89] However, violent rockbursts may occasionally appear as unpredictable "black-swans" (a metaphor for rare, high-impact events that come as a surprise).[90] These black-swan events may result from unstable rupture along blast-generated inward-dipping fractures (i.e., inclined toward the stope face), where the stored strain energy cannot be sufficiently dissipated in advance.[15] This contrasts with the more stable creep behavior along blast-generated outward-dipping fractures (i.e., inclined away from the stope face, as illustrated in Fig. 1b),[16] where part of the stored strain energy can be gradually dissipated, often accompanied by identifiable precursory signals, prior to an eventual failure. It is also conjectured that black-swan rockbursts are more likely to occur in strong, brittle rock formations where limited deformation precedes failure, whereas dragon-king rockbursts tend to develop in more ductile settings that allow for progressive deformation and energy dissipation. This aligns with past extensive field observations in South African gold and platinum mines: in brittle, high-strength rocks such as Ventersdorp lavas and quartzites (with uniaxial compression strengths exceeding 400 MPa and 250 MPa, respectively), stope closure monitoring rarely revealed precursory acceleration before large seismic events. In contrast, in more ductile platinum mine settings (where the rock's uniaxial compression strength is typically below 150 MPa), sustained stable closure can be observed and may allow the detection of precursors. Black-swan scenarios pose greater challenges for monitoring and forecasting compared to endogenously driven dragon-king cases; however, acknowledging the limits of predictability is itself a valuable insight.

5. Conclusions

To conclude, we have developed a novel endo-exo theoretical framework to quantitatively diagnose episodic creep events in deep underground rock masses, capturing the interplay between external triggers (such as blasting and excavation) and internal processes (such as damage and healing). Our framework classifies episodic dynamics into four fundamental types, defined by the origin of disturbance (endogenous or exogenous) and the level of criticality (subcritical or critical), which are all governed by a single parameter θ, which controls the four distinct temporal power law regimes surrounding a velocity peak. Through a mean-field formulation that integrates fundamental endo-exo mechanisms and upscales individual block interactions to global rock mass dynamics, our model functions as a parsimonious tool, effectively capturing the macroscopic behavior of rock masses at the site scale while retaining the flexibility required for empirical calibration. Unlike many numerical simulations that require diagnostic tests on rock samples for validation or calibration, which is often faced with challenges in upscaling lab-scale measurements to the site scale, our model can be directly applied to field data. We have tested and validated our framework using the comprehensive monitoring data of a platinum mine in South Africa. The parameter θ for this mine was estimated to be around 0.35, which we interpret as reflecting persistent stress fluctuations arising from anomalous diffusion processes or bursty stress redistributions that drive episodic rock mass movements and interactions. Our parsimonious framework points at the existence of a deep quantitative relationship between episodic dynamics, external triggers, and internal processes in rock masses. This framework enables us to differentiate between endogenous and exogenous origins of rock creep responses, while also shedding light on their underlying physical mechanisms and their connection to catastrophic failures. Our findings provide critical insights into the fundamental mechanisms of episodic creep movements in rock masses and pave the way for enhanced rockburst hazard prediction and mitigation in deep underground mining environments. Our results also have broad implications for understanding similar episodic phenomena in other geophysical systems such as fault slow slip, landslide creep, volcanic unrest, and glacier surge.

CRediT authorship contribution statement

Qinghua Lei: Writing – original draft, Visualization, Validation, Software, Resources, Project administration, Methodology, Investigation, Funding acquisition, Formal analysis, Conceptualization. **Daniel Francois Malan:** Writing – review & editing, Methodology, Data curation. **Didier Sornette:** Writing – review & editing, Methodology, Investigation, Funding acquisition, Conceptualization.

Declaration of competing interest

The authors declare that they have no known competing financial interests or personal relationships that could have appeared to influence the work reported in this paper.

Acknowledgement

Q.L. is grateful for the support from the Swedish Rock Engineering Research Foundation and the State Key Laboratory of Intelligent Coal Mining and Strata Control. D.S. acknowledges partial support by the National Natural Science Foundation of China (Grant no. T2350710802, U2039202), and the Center for Computational Science and Engineering at Southern University of Science and Technology. Q.L. acknowledges the National Academic Infrastructure for Supercomputing in Sweden (NAISS), partially funded by the Swedish Research Council through grant agreement no. 2022–06725, for awarding this project access to the LUMI supercomputer, owned by the EuroHPC Joint Undertaking and hosted by CSC (Finland) and the LUMI consortium.

Appendix A. Supplementary data

Supplementary data to this article can be found online at https://doi.org/10.1016/j.ijrmms.2025.106251.

Data availability

Data will be made available on request.

References

1. International Energy Agency. The role of critical minerals in clean energy transitions. In: *World Energy Outlook*. International Energy Agency; 2021.
2. Cook NGW. A note on rockbursts considered as a problem of stability. *J South Afr Inst Min Metall*. 1965;65(8):437–446.
3. Cook NGW. The failure of rock. *Int J Rock Mech Min Sci Geomech Abstr*. 1965;2(4):389–403. https://doi.org/10.1016/0148-9062(65)90004-5.
4. Salamon MDG. Stability, instability and design of pillar workings. *Int J Rock Mech Min Sci Geomech Abstr*. 1970;7(6):613–631. https://doi.org/10.1016/0148-9062(70)90022-7.
5. Cook NGW. Seismicity associated with mining. *Eng Geol*. 1976;10(2-4):99–122. https://doi.org/10.1016/0013-7952(76)90015-6.
6. Vardoulakis I. Rock bursting as a surface instability phenomenon. *Int J Rock Mech Min Sci Geomech Abstr*. 1984;21(3):137–144. https://doi.org/10.1016/0148-9062(84)91531-6.
7. Linkov AM. Rockbursts and the instability of rock masses. *Int J Rock Mech Min Sci Geomech Abstr*. 1996;33(7):727–732. https://doi.org/10.1016/0148-9062(96)00021-6.
8. Ortlepp WD, Stacey TR. Rockburst mechanisms in tunnels and shafts. *Tunn Undergr Space Technol*. 1994;9(1):59–65. https://doi.org/10.1016/0886-7798(94)90010-8.
9. Ranjith PG, Zhao J, Ju M, De Silva RVS, Rathnaweera TD, Bandara AKMS. Opportunities and challenges in deep mining: a brief review. *Engineering*. 2017;3(4):546–551. https://doi.org/10.1016/J.ENG.2017.04.024.

10. Cai M. Rockburst risk control and mitigation in deep mining. *Deep Resour Eng*. 2024; 1(2), 100019. https://doi.org/10.1016/j.deepre.2024.100019.
11. Hsiung SM, Blake W, Chowdhury AH, Williams TJ. Effects of mining-induced seismic events on a deep underground mine. *Pure Appl Geophys*. 1992;139(3-4): 741–762. https://doi.org/10.1007/BF00879961.
12. Malan DF. Time-dependent behaviour of deep level tabular excavations in hard rock. *Rock Mech Rock Eng*. 1999;32(2):123–155. https://doi.org/10.1007/s006030050028.
13. Malan DF, Napier JAL, Janse van Rensburg AL. Stope deformation measurements as a diagnostic measure of rock behaviour: a decade of research. *J South Afr Inst Min Metall*. 2007;107:743–765.
14. Malan DF, Napier JAL. A review of the role of underground measurements in the historical development of rock engineering in South Africa. *J South Afr Inst Min Metall*. 2021;121(5):201–216. https://doi.org/10.17159/2411-9717/1443/2021.
15. McGarr A. Violent deformation of rock near deep-level, tabular excavations—Seismic events. *Bull Seismol Soc Am*. 1971;61(5):1453–4166. https://doi.org/10.1785/BSSA0610051453.
16. McGarr A. Stable deformation of rock near deep-level tabular excavations. *J Geophys Res*. 1971;76(29):7088–7106. https://doi.org/10.1029/JB076i029p07088.
17. McGarr A, Sacks IS, Linde AT, Spottiswoode SM, Green RWE. Coseismic and other short-term strain changes recorded with Sacks-Evertson strainmeters in a deep mine, South Africa. *Geophys J Int*. 1982;70(3):717–740. https://doi.org/10.1111/j.1365-246X.1982.tb05980.x.
18. McGarr A, Green RWE. Measurement of tilt in a deep-level gold mine and its relationship to mining and seismicity. *Geophys J Int*. 1975;43(2):327–345. https://doi.org/10.1111/j.1365-246X.1975.tb00638.x.
19. Walsh JB, Leyde EE, White AJA, Carragher BL. Stope closure studies at West Driefontein Gold Mine. *Int J Rock Mech Min Sci Geomech Abstr*. 1977;14(5-6): 277–281. https://doi.org/10.1016/0148-9062(77)90738-0.
20. Lei Q, Sornette D. Oscillatory finite-time singularities in rockbursts. *Int J Rock Mech Min Sci*. 2025;192, 106156. https://doi.org/10.1016/j.ijrmms.2025.106156.
21. Lei Q, Sornette D. Unified failure model for landslides, rockbursts, glaciers, and volcanoes. *Commun Earth Environ*. 2025;6:390. https://doi.org/10.1038/s43247-025-02369-z.
22. Ouillon G, Sornette D. The concept of “critical earthquakes” applied to mine rockbursts with time-to-failure analysis. *Geophys J Int*. 2000;143(2):454–468. https://doi.org/10.1046/j.1365-246X.2000.01257.x.
23. Askaripour M, Saeidi A, Rouleau A, Mercier-Langevin P. Rockburst in underground excavations: a review of mechanism, classification, and prediction methods. *Undergr Space*. 2022;7(4):577–607. https://doi.org/10.1016/j.undsp.2021.11.008.
24. He M, Cheng T, Qiao Y, Li H. A review of rockburst: experiments, theories, and simulations. *J Rock Mech Geotech Eng*. 2023;15(5):1312–1353. https://doi.org/10.1016/j.jrmge.2022.07.014.
25. Sornette D, Helmstetter A. Endogenous versus exogenous shocks in systems with memory. *Physica A Stat Mech Appl*. 2003;318(3-4):577–591. https://doi.org/10.1016/S0378-4371(02)01371-7.
26. Helmstetter A, Sornette D. Subcritical and supercritical regimes in epidemic models of earthquake aftershocks. *J Geophys Res*. 2002;107(B10). https://doi.org/10.1029/2001JB001580.
27. Helmstetter A, Sornette D, Grasso J. Mainshocks are aftershocks of conditional foreshocks: how do foreshock statistical properties emerge from aftershock laws. *J Geophys Res*. 2003;108(B1), 2002JB001991. https://doi.org/10.1029/2002JB001991.
28. Lei Q, Sornette D. Endo-exo framework for a unifying classification of episodic landslide movements: Implications for forecasting catastrophic failures. *Sci. Adv*. 2025. https://doi.org/10.1126/sciadv.ady9141.
29. Sornette D. Endogenous versus exogenous origins of crises. In: Albeverio S, Jentsch V, Kantz H, eds. *Extreme Events in Nature and Society*. Springer; 2006:95–119. https://doi.org/10.1007/3-540-28611-X_5.
30. Scholz CH. *The Mechanics of Earthquakes and Faulting*. third ed. Cambridge University Press; 2019. https://doi.org/10.1017/9781316681473.
31. Sahoo S, Kundu B, Petrosino S, Yadav RK, Tiwari DK, Jin S. Feedback responses between endogenous and exogenous processes at Campi Flegrei caldera dynamics, Italy. *Bull Volcanol*. 2024;86(3):22. https://doi.org/10.1007/s00445-024-01719-7.
32. Lacroix P, Handwerger AL, Bièvre G. Life and death of slow-moving landslides. *Nat Rev Earth Environ*. 2020;1(8):404–419. https://doi.org/10.1038/s43017-020-0072-8.
33. Giordan D, Dematteis N, Allasia P, Motta E. Classification and kinematics of the Planpincieux Glacier break-offs using photographic time-lapse analysis. *J Glaciol*. 2020;66(256):188–202. https://doi.org/10.1017/jog.2019.99.
34. Wang L, Lei Q. Modelling rockbursts around a deep tunnel based on the particle finite element method: from progressive degradation to catastrophic ejection. *Int J Rock Mech Min Sci*. 2025;191, 106131. https://doi.org/10.1016/j.ijrmms.2025.106131.
35. Jager AJ, Ryder JA. A handbook on rock engineering practice for tabular hard rock mines. *Safety in Mines Research Advisory Committee*. 1999.
36. Malan DF, Napier JAL. Rockburst support in shallow-dipping tabular stopes at great depth. *Int J Rock Mech Min Sci*. 2018;112:302–312. https://doi.org/10.1016/j.ijrmms.2018.10.026.
37. Jooste Y, Napier JAL, Malan DF. A bulking model to simulate stope convergence in deep tabular excavations. *Int J Rock Mech Min Sci*. 2023;170, 105480. https://doi.org/10.1016/j.ijrmms.2023.105480.
38. Jaeger JC, Cook NGW, Zimmerman RW. *Fundamentals of Rock Mechanics*. fourth ed. Wiley-Blackwell; 2007.
39. Burridge R, Knopoff L. Model and theoretical seismicity. *Bull Seismol Soc Am*. 1967; 57(3):341–371. https://doi.org/10.1785/BSSA0570030341.
40. Rundle JB, Turcotte DL, Shcherbakov R, Klein W, Sammis C. Statistical physics approach to understanding the multiscale dynamics of earthquake fault systems. *Rev Geophys*. 2003;41(4), 2003RG000135. https://doi.org/10.1029/2003RG000135.
41. Goodman RE. Block theory and its application. *Geotechnique*. 1995;45(3):383–423. https://doi.org/10.1680/geot.1995.45.3.383.
42. Brantut N, Heap MJ, Meredith PG, Baud P. Time-dependent cracking and brittle creep in crustal rocks: a review. *J Struct Geol*. 2013;52:17–43. https://doi.org/10.1016/j.jsg.2013.03.007.
43. Marone C. Laboratory-derived friction laws and their application to seismic faulting. *Annu Rev Earth Planet Sci*. 1998;26(1):643–696. https://doi.org/10.1146/annurev.earth.26.1.643.
44. Andrade ENDC. On the viscous flow in metals, and allied phenomena. *Proc Roy Soc Lond A*. 1910;84(567):1–12. https://doi.org/10.1098/rspa.1910.0050.
45. Utsu T, Ogata Y, S R, Matsu’ura. The centenary of the omori formula for a decay law of aftershock activity. *J Phys Earth*. 1995;43(1):1–33. https://doi.org/10.4294/jpe1952.43.1.
46. Shaw BE. Generalized omori law for aftershocks and foreshocks from a simple dynamics. *Geophys Res Lett*. 1993;20(10):907–910. https://doi.org/10.1029/93GL01058.
47. Dieterich J. A constitutive law for rate of earthquake production and its application to earthquake clustering. *J Geophys Res*. 1994;99(B2):2601–2618. https://doi.org/10.1029/93JB02581.
48. Nechad H, Helmstetter A, El Guerjouma R, Sornette D. Andrade and critical time-to-failure laws in fiber-matrix composites: experiments and model. *J Mech Phys Solid*. 2005;53(5):1099–1127. https://doi.org/10.1016/j.jmps.2004.12.001.
49. Kagan YY, Knopoff L. Stochastic synthesis of earthquake catalogs. *J Geophys Res*. 1981;86(B4):2853–2862. https://doi.org/10.1029/JB086iB04p02853.
50. Perfettini H, Avouac J-P. Postseismic relaxation driven by brittle creep: a possible mechanism to reconcile geodetic measurements and the decay rate of aftershocks, application to the chi-chi earthquake, Taiwan. *J Geophys Res*. 2004;109(B2), 2003JB002488. https://doi.org/10.1029/2003JB002488.
51. Freed AM, Lin J. Delayed triggering of the 1999 hector mine earthquake by viscoelastic stress transfer. *Nature*. 2001;411(6834):180–183. https://doi.org/10.1038/35075548.
52. Lindman M, Lund B, Roberts R, Jonsdottir K. Physics of the omori law: inferences from interevent time distributions and pore pressure diffusion modeling. *Tectonophysics*. 2006;424(3):209–222. https://doi.org/10.1016/j.tecto.2006.03.045.
53. Hirata T. Omori’s power law aftershock sequences of microfracturing in rock fracture experiment. *J Geophys Res*. 1987;92(B7):6215–6221. https://doi.org/10.1029/JB092iB07p06215.
54. Hawkes AG, Oakes D. A cluster process representation of a self-exciting process. *J Appl Probab*. 1974;11(3):493–503. https://doi.org/10.2307/3212693.
55. Harris TE. *The Theory of Branching Processes*. Springer; 1963.
56. Sornette D. *Critical Phenomena in Natural Sciences - Chaos, Fractals, Selforganization and Disorder: Concepts and Tools*. Springer; 2006. https://doi.org/10.1007/3-540-33182-4.
57. Sornette D, Helmstetter A. Occurrence of finite-time singularities in epidemic models of rupture, earthquakes, and starquakes. *Phys Rev Lett*. 2002;89(15), 158501. https://doi.org/10.1103/PhysRevLett.89.158501.
58. Saichev A, Helmstetter A, Sornette D. Power-law distributions of offspring and generation numbers in branching models of earthquake triggering. *Pure Appl Geophys*. 2005;162(6-7):1113–1134. https://doi.org/10.1007/s00024-004-2663-6.
59. Malan DF. *An Investigation into the Identification and Modelling of Time-dependent Behaviour of Deep Level Excavations in Hard Rock*. University of the Witwatersrand; 1998.
60. Kagan YY, Knopoff L. Random stress and earthquake statistics: time dependence. *Geophys J Int*. 1987;88(3):723–731. https://doi.org/10.1111/j.1365-246X.1987.tb01653.x.
61. Mandelbrot BB, Van Ness JW. Fractional Brownian motions, fractional noises and applications. *SIAM Rev*. 1968;10(4):422–437. https://doi.org/10.1137/1010093.
62. Rangarajan G, Ding M. Anomalous diffusion and the first passage time problem. *Phys Rev E*. 2000;62(1):120–133. https://doi.org/10.1103/PhysRevE.62.120.
63. Rosso A, Zoia A. First passage problems in anomalous diffusion. In: *First-Passage Phenomena and their Applications*. World Scientific; 2014:45–69. https://doi.org/10.1142/9789814590297_0003.
64. McGarr A, Wiebols GA. Influence of mine geometry and closure volume on seismicity in a deep-level mine. *Int J Rock Mech Min Sci Geomech Abstr*. 1977;14(3): 139–145. https://doi.org/10.1016/0148-9062(77)90005-5.
65. Lucier AM, Zoback MD, Heesakkers V, Reches Z, Murphy SK. Constraining the far-field in situ stress state near a deep South African gold mine. *Int J Rock Mech Min Sci*. 2009;46(3):555–567. https://doi.org/10.1016/j.ijrmms.2008.09.005.
66. McGarr A. Energy budgets of mining-induced earthquakes and their interactions with nearby stopes. *Int J Rock Mech Min Sci*. 2000;37(1-2):437–443. https://doi.org/10.1016/S1365-1609(99)00118-5.
67. Chechkin AV, Gonchar VY, Klafter J, Metzler R. Fundamentals of lévy flight processes. In: Coffey WT, Kalmykov YP, eds. *Advances in Chemical Physics*. first ed. Wiley; 2006:439–496. https://doi.org/10.1002/0470037148.ch9.
68. Redner S. *A Guide to First-Passage Processes*. first ed. Cambridge University Press; 2001. https://doi.org/10.1017/CBO9780511606014.
69. Nandan S, Ram SK, Ouillon G, Sornette D. Is seismicity operating at a critical point? *Phys Rev Lett*. 2021;126(12), 128501. https://doi.org/10.1103/PhysRevLett.126.128501.
70. Bak P. *How Nature Works: The Science of Self-Organized Criticality*. Springer; 1996. https://doi.org/10.1007/978-1-4757-5426-1.

71. Cowie PA, Vanneste C, Sornette D. Statistical physics model for the spatiotemporal evolution of faults. *J Geophys Res*. 1993;98(B12):21809–21821. https://doi.org/10.1029/93JB02223.
72. Sornette D, Miltenberger P, Vanneste C. Statistical physics of fault patterns self-organized by repeated earthquakes. *Pure Appl Geophys*. 1994;142(3-4):491–527. https://doi.org/10.1007/BF00876052.
73. Malan DF. Simulating the time-dependent behaviour of excavations in hard rock. *Rock Mech Rock Eng*. 2002;35(4):225–254. https://doi.org/10.1007/s00603-002-0026-0.
74. Voight B. A method for prediction of volcanic eruptions. *Nature*. 1988;332(6160):125–130. https://doi.org/10.1038/332125a0.
75. Voight B. A relation to describe rate-dependent material failure. *Science*. 1989;243(4888):200–203. https://doi.org/10.1126/science.243.4888.200.
76. Intrieri E, Carlà T, Gigli G. Forecasting the time of failure of landslides at slope-scale: a literature review. *Earth Sci Rev*. 2019;193:333–349. https://doi.org/10.1016/j.earscirev.2019.03.019.
77. Kilburn C. Precursory deformation and fracture before brittle rock failure and potential application to volcanic unrest. *J Geophys Res*. 2012;117(B2), 2011JB008703. https://doi.org/10.1029/2011JB008703.
78. Main IG. Applicability of time-to-failure analysis to accelerated strain before earthquakes and volcanic eruptions. *Geophys J Int*. 1999;139(3):F1–F6. https://doi.org/10.1046/j.1365-246x.1999.00004.x.
79. Nemat-Nasser S, Horii H. Compression-induced nonplanar crack extension with application to splitting, exfoliation, and rockburst. *J Geophys Res*. 1982;87(B8):6805–6821. https://doi.org/10.1029/JB087iB08p06805.
80. Sammis CG, Sornette D. Positive feedback, memory, and the predictability of earthquakes. *Proc Natl Acad Sci*. 2002;99(suppl_1):2501–2508. https://doi.org/10.1073/pnas.012580999.
81. Helmstetter A, Sornette D, Grasso J-R, Andersen JV, Gluzman S, Pisarenko V. Slider block friction model for landslides: application to Vaiont and La Clapière landslides. *J Geophys Res*. 2004;109(B2), 2002JB002160. https://doi.org/10.1029/2002JB002160.
82. Noda H, Chang C. Tertiary creep behavior for various rate- and state-dependent friction laws. *Earth Planet Sci Lett*. 2023;619, 118314. https://doi.org/10.1016/j.epsl.2023.118314.
83. McGarr A, Spottiswoode SM, Gay NC. Relationship of mine tremors to induced stresses and to rock properties in the focal region. *Bull Seismol Soc Am*. 1975;65(4):981–993. https://doi.org/10.1785/BSSA0650040981.
84. McGarr A, Spottiswoode SM, Gay NC, Ortlepp WD. Observations relevant to seismic driving stress, stress drop, and efficiency. *J Geophys Res*. 1979;84(B5):2251–2261. https://doi.org/10.1029/JB084iB05p02251.
85. Spottiswoode SM, McGarr A. Source parameters of tremors in a deep-level gold mine. *Bull Seismol Soc Am*. 1975;65(1):93–112. https://doi.org/10.1785/BSSA0650010093.
86. Richardson E. Seismicity in deep gold mines of South Africa: implications for tectonic earthquakes. *Bull Seismol Soc Am*. 2002;92(5):1766–1782. https://doi.org/10.1785/0120000226.
87. Sornette D. Predictability of catastrophic events: material rupture, earthquakes, turbulence, financial crashes, and human birth. *Proc Natl Acad Sci*. 2002;99(suppl_1):2522–2529. https://doi.org/10.1073/pnas.022581999.
88. Sornette D, Ouillon G. Dragon-kings: mechanisms, statistical methods and empirical evidence. *Eur Phys J Spec Top*. 2012;205(1):1–26. https://doi.org/10.1140/epjst/e2012-01559-5.
89. Lei Q, Sornette D, Yang H, Loew S. Real-time forecast of catastrophic landslides via dragon-king detection. *Geophys Res Lett*. 2023;50(6), e2022GL100832. https://doi.org/10.1029/2022GL100832.
90. Taleb NN. *The Black Swan: The Impact of the Highly Improbable*. Penguin; 2010.